




# An All-Aqueous Thermally Regenerative Ammonia Battery Chemistry Using Cu(I, II) Redox Reactions

Renaldo Springer,<sup>1,2</sup> Nicholas R. Cross,<sup>3,\*</sup> Serguei N. Lvov,<sup>1,2,4</sup> Bruce E. Logan,<sup>3,5</sup> Christopher A. Gorski,<sup>5</sup> and Derek M. Hall<sup>1,2,\*\*,z</sup> 

<sup>1</sup>The EMS Energy Institute, The Pennsylvania State University, University Park, Pennsylvania, United States of America

<sup>2</sup>Department of Energy and Mineral Engineering, The Pennsylvania State University, University Park, Pennsylvania, United States of America

<sup>3</sup>Department of Chemical Engineering, The Pennsylvania State University, University Park, Pennsylvania, United States of America

<sup>4</sup>Department of Materials Science and Engineering, The Pennsylvania State University, University Park, Pennsylvania, United States of America

<sup>5</sup>Department of Civil and Environmental Engineering, The Pennsylvania State University, University Park, Pennsylvania, United States of America

Thermally regenerative ammonia batteries (TRABs) are electrochemical energy conversion devices that convert low-grade waste heat into electrical power. To date, reported TRABs have suffered from poor performance due to their reliance on dissolution and deposition redox reactions with transition metals. Here we present a new TRAB chemistry that uses ligands to stabilize aqueous Cu(I) and Cu(II) ions, thereby creating the first reported all-aqueous TRAB. Rotating disc electrode studies were conducted to evaluate thermodynamic and kinetic parameters of prospective anolyte and catholyte chemistries. The use of  $\text{NH}_3(\text{aq})$  and  $\text{Br}^-(\text{aq})$  ligands resulted in a cell potential difference of  $695 \pm 2$  mV with rate constants of  $101 \pm 5 \mu\text{m s}^{-1}$  and  $819 \pm 236 \mu\text{m s}^{-1}$ , respectively. Single-cell tests achieved power densities up to  $350 \text{ W m}^{-2}$  which are the highest reported for single metal TRABs at  $25^\circ\text{C}$ . Coulombic efficiencies exceeded 90% and their energy storage densities were two to four times of those reported for alternative TRAB chemistries.

© 2021 The Electrochemical Society ("ECS"). Published on behalf of ECS by IOP Publishing Limited. [DOI: [10.1149/1945-7111/ac1030](https://doi.org/10.1149/1945-7111/ac1030)]

Manuscript submitted July 20, 2020; revised manuscript received June 1, 2021. Published July 13, 2021.

Supplementary material for this article is available [online](#)

Low-grade waste heat (temperatures  $<130^\circ\text{C}$ ) remains an untapped energy source, as heat recovery technologies still struggle with poor performance.<sup>1–3</sup> Equating to approximately half of the U.S. current energy demand ( $2.94 \times 10^{13}$  kWh in 2019),<sup>4</sup> harvesting a fraction of this low-grade waste heat would alleviate  $\text{CO}_2$  emissions from the combustion of additional fossil fuels, thereby promoting a more sustainable energy infrastructure.<sup>1,2,5,6</sup> Solid-state thermoelectric devices, such as the thermoelectric generator (TEG), can convert heat flux to electric power based on the Seebeck effect,<sup>7,8</sup> but their high manufacturing costs and low power densities hinder practical applications.<sup>1,9,10</sup> Liquid-based thermoelectric cells are better candidates for efficiently harvesting waste heat due to more appealing costs and scalability.<sup>11</sup> However, with power densities ranging from  $0.5$  to  $12 \text{ W m}^{-2}$ , power generation and efficiency improvements are still needed.<sup>5,10</sup>

Thermally regenerative ammonia batteries (TRABs) are a promising option for converting waste heat into electric power compared to competing technologies, but they still have issues such as low energy storage densities and poor coulombic efficiencies.<sup>2,5,12</sup> Unlike alternative approaches to waste heat recovery, TRABs can store harvested thermal energy by using ammonia as an energy carrier.<sup>2</sup> During TRAB cell discharge, a metal anode is oxidized and metal amine complexes are formed, whereas aqueous metal ions deposit at the cathode in the absence of ammonia.<sup>5</sup> Thermal recovery of the potential difference is accomplished by separating ammonia from the depleted anolyte through distillation and re-introducing the recovered ammonia to the former cathode chamber, regenerating the potential difference.<sup>2,5,13</sup> This results in a closed cycle that uses heat as an input, which is stored in the energy carrier (ammonia) and provides electric energy as an output. The power densities from TRABs using commercial membranes and electrode materials were  $\sim 30 \text{ W m}^{-2}$  which was still substantially larger than other emerging electrochemical and

membrane-based heat recovery technologies.<sup>5,14,15</sup> Using novel membrane and electrode materials, Cu-based TRABs have achieved power densities up to  $280 \text{ W m}^{-2}$  at  $55^\circ\text{C}$ , albeit with coulombic efficiencies under 50%.<sup>2</sup> Recently, a Cu/Zn-TRAB reported a power density of  $723 \pm 45 \text{ W m}^{-2}$  at  $40^\circ\text{C}$  with a linear temperature relationship of  $12.25 \text{ W m}^{-2} \text{ }^\circ\text{C}^{-1}$ .<sup>16</sup> In terms of energy storage densities, Ag-based and Cu-based TRABs use active species concentrations between  $0.1$  to  $0.2 \text{ M}$  with equilibrium potential differences between  $0.4$  to  $0.45 \text{ V}$ ,<sup>2,5</sup> resulting in energy storage densities between  $1$  to  $3 \text{ Wh L}^{-1}$ . A major disadvantage of these previous technologies is their dependence on deposition reactions, which can lead to dendrite formation, limiting practical applications.

Here, we present a new all-aqueous TRAB that uses ligands to stabilize Cu(I) ions in the anolyte and catholyte chambers which increases the coulombic efficiency, power density, and energy density of copper-based TRABs by avoiding their reliance on thermodynamically unstable deposition and dissolution reactions. A rotating disc electrode (RDE) system was used to examine how three ligands that readily complex with Cu(I) and Cu(II), influence the electrochemical parameters of the Cu(I, II) redox reaction. Full cell tests were performed to determine peak power densities and coulombic efficiencies of this new TRAB chemistry using a conventional zero-gap flow battery system with graphite felt electrodes.

## Materials, Techniques, and Calculations

**Materials and reagents.**—Electrolyte solutions were prepared using ammonium chloride (99.5% Alfa Aesar), ammonium bromide (99% Alfa Aesar), and copper chloride dihydrate (99% Alfa Aesar) salts. Ammonium hydroxide was prepared from a 28% wt. ammonia Alfa Aesar stock solution. The chemical conversion of Cu(II) complexes to Cu(I) was carried out under an argon gas blanket (99.998% Praxair), following a procedure developed previously.<sup>17,18</sup> Briefly, an electrolyte containing Cu(II) complexes with a ligand that then stabilizes the formation of Cu(I) is circulated with Cu(s) (99.9% Alfa Aesar metal basis), promoting the formation of Cu(I) complexes through the consumption of Cu(s) and  $\text{Cu}^{2+}(\text{aq})$ .

\*Electrochemical Society Student Member

\*\*Electrochemical Society Member

<sup>z</sup>E-mail: [hall@psu.edu](mailto:hall@psu.edu)

**Cell assemblies.**—Analysis of ligand impacts on the electrochemical parameters of the Cu(I, II) redox couple was conducted using a Pine Instruments rotating disc electrode (RDE) system and a multiport glass cell (#AKCELL2). The RDE test system consisted of an Ag/AgCl reference electrode (RE) with a 4 mol kg<sup>-1</sup> KCl(aq) reference solution, and the counter electrode (CE) was a platinum coil. The two working electrodes used were platinum (Pt) and glassy carbon (GC) Fixed-Disk RDE Tips (Pine Instruments), both having a surface area of 0.1964 cm<sup>2</sup>. Both working electrodes were polished with an alumina polishing solution (0.05 μm Buehler) on a microfiber felt and rinsed with deionized (DI) water before each test. All RDE tests were performed using 10 × 10<sup>-3</sup> mol kg<sup>-1</sup> Cu(I) species and 10 × 10<sup>-3</sup> mol kg<sup>-1</sup> Cu(II) species. Ligand concentrations were varied between 1 and 4 mol kg<sup>-1</sup>. Additional details about the system and approach used were published previously.<sup>19</sup>

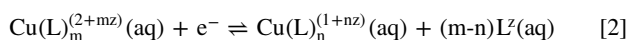
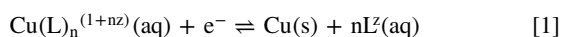
The full cell performance studies used a zero-gap flow battery cell. The zero-gap cell had machined graphite plates with 5 cm<sup>2</sup> serpentine flow channels, steel endplates, carbon cloth electrodes, ion-conductive membranes, and fluorosilicone gaskets (Fig. 1).

The membranes examined were Nafion 117 (183 μm thick), Nafion 115 (127 μm thick) and a Fumasep FAPQ-375-PP anion exchange membrane (68–82 μm thick) (AEM). To pump the electrolytes, two Masterflex diaphragm pumps with a combination of perfluoroalkoxy (PFA) and polytetrafluoroethylene (PTFE) tubing and fittings were used. The electrolyte solutions were pumped at a constant flow rate (200 ml min<sup>-1</sup>) into the cell through the flow channels then back into 1-liter reservoir tanks. This flow rate value was selected based on previous studies<sup>17,20</sup> to minimize conversion within the system to demonstrate the power density at a given state of charge. In all full cell tests, the positive electrode electrolytes contained 5 mol kg<sup>-1</sup> NH<sub>4</sub>Br with Cu(I, II) bromide complexes, and the negative electrode electrolytes contained 5 mol kg<sup>-1</sup> NH<sub>4</sub>Br and 5 mol kg<sup>-1</sup> NH<sub>3</sub> with Cu(I, II) ammonia complexes (Fig. 2). Initial copper concentrations for both positive and negative electrolytes were 0.5 mol kg<sup>-1</sup>.

The initial state of charge (SOC) was controlled through the mixing of Cu(I) with Cu(II) solutions, using an approach developed in our laboratory for the CuCl-HCl electrolyzer.<sup>17,18,21</sup>

**Test parameters.**—Experimental measurements were performed with a Gamry Reference 600 for RDE tests and a Gamry Reference 3000 for full cell tests. The tests consisted of open circuit potential (OCP), linear sweep voltammetry (LSV), and electrochemical impedance spectroscopy (EIS) measurements. RDE LSV data were collected with a scan rate of 10 mV s<sup>-1</sup> from potentials ±0.3 V vs OCP while full cell LSV data were obtained using a scan rate of 5 mV s<sup>-1</sup>. LSV data collected from the RDE system were corrected for the solution resistance, obtained via EIS, to examine the overpotential (η) contributions from electrode reaction processes. EIS tests used a frequency range of 0.1 Hz to 100 kHz, sampling every 5 points per decade with a 10 mV root mean square (RMS) alternating current perturbation around the OCP. Tests were conducted around OCP to minimize non-linear kinetic responses at applied potentials. Cycling tests were performed at a constant current of 40 A m<sup>-2</sup> with potential limits of 1 and 0.5 V.

**Thermodynamics.**—Using stability constants (β) for each copper-ligand complex, the standard values of the electrode potentials, E<sup>0</sup>, values were calculated for the Cu(I, 0) and Cu(I, II) redox reactions (Eqs. 1 and 2) where L is the ligand molecule, z is the charge number of the ligand, and n and m are the stoichiometric coefficients of the ligands in the Cu(I) and Cu(II) complexation reactions, respectively.



The new values (E<sup>0</sup><sub>Cu(I)L/Cu(0)</sub> and E<sup>0</sup><sub>Cu(II)L/Cu(I)L</sub>) were calculated from the standard E<sup>0</sup> values reported in the CRC electrochemical

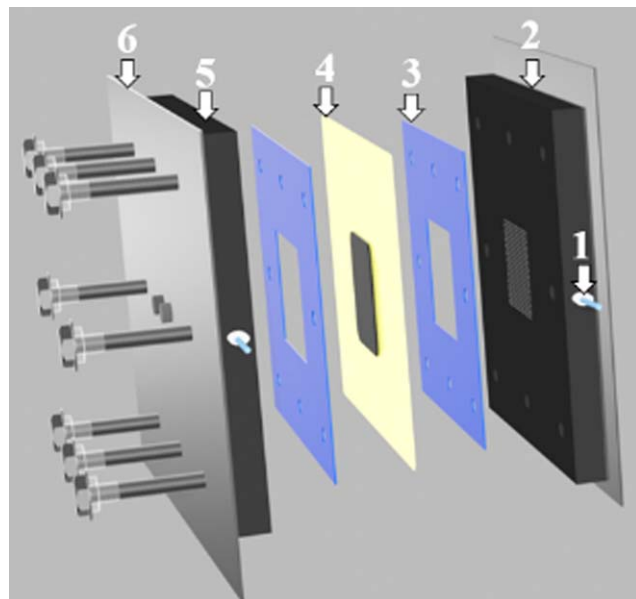


**Figure 1.** Model of RFB used for full cell testing: (1) electrolyte inlet and outlet; (2) negative electrode current collector; (3) fluorosilicone gasket; (4) ion-conductive membrane with carbon cloth electrodes; (5) positive electrode current collector; (6) steel endplate.

series<sup>22</sup> (E<sup>0</sup><sub>Cu(II)/Cu(I)</sub> = 0.153 V vs SHE and E<sup>0</sup><sub>Cu(I)/Cu(0)</sub> = 0.342 V vs SHE), and the stability constants, β<sub>n</sub> and β<sub>m</sub>, for the Cu(I)L<sub>n</sub> and Cu(II)L<sub>m</sub> reactions.

$$E^0_{\text{Cu(I)L/Cu(0)}} = E^0_{\text{Cu(I)/Cu(0)}} - \frac{RT}{F} \ln(\beta_n) \quad [3]$$

$$E^0_{\text{Cu(II)L/Cu(I)L}} = E^0_{\text{Cu(II)/Cu(I)}} + \frac{RT}{F} \ln(\beta_n \beta_m^{-1}) \quad [4]$$

where  $F = 96485 \text{ C mol}^{-1}$  is Faraday's constant,  $R = 8.314 \text{ J mol}^{-1}\text{K}^{-1}$  is the molar gas constant and  $T$  is the thermodynamic temperature in K.

The stability constants for copper(I,II) complexes were obtained from literature based on complexation reactions.<sup>23–25</sup> All potential values provided vs SHE. The coulombic efficiency (ε<sub>C</sub>) of the Br-NH<sub>3</sub> all-aq TRB was determined from a series of charge and discharge cycles at a constant current (Eq. 5):<sup>26</sup>

$$\epsilon_C = \frac{\int I dt_{\text{charge}}}{\int I dt_{\text{discharge}}} \quad [5]$$

where  $I$  is the cell constant current of charge and discharge for a period of time,  $t$ , between the potential limits, 0.5 to 1.0 V, of the cycling tests. Theoretical energy storage density ( $U_{\text{ideal}}$ ) calculations were made following a simplified approximation which neglects potential cut-offs and activity coefficient effects<sup>27</sup> to compare the energy capacity of multiple TRAB chemistries:

$$U_{\text{ideal}} = E^0_{\text{cell}} c_{\text{total}} F \quad [6]$$

where  $E^0_{\text{cell}}$  is the difference between the standard potentials of the redox reaction of interest in each half of the battery, and  $c_{\text{total}}$  is the concentration of the electroactive species limiting the state of charge.<sup>27</sup> For this TRAB chemistry,  $c_{\text{total}}$  is the total concentration of dissolved copper.

## Results and Discussion

**Thermodynamic analysis.**—A thermodynamic analysis of the Cu (I, II) redox reaction with different ligands indicated that the

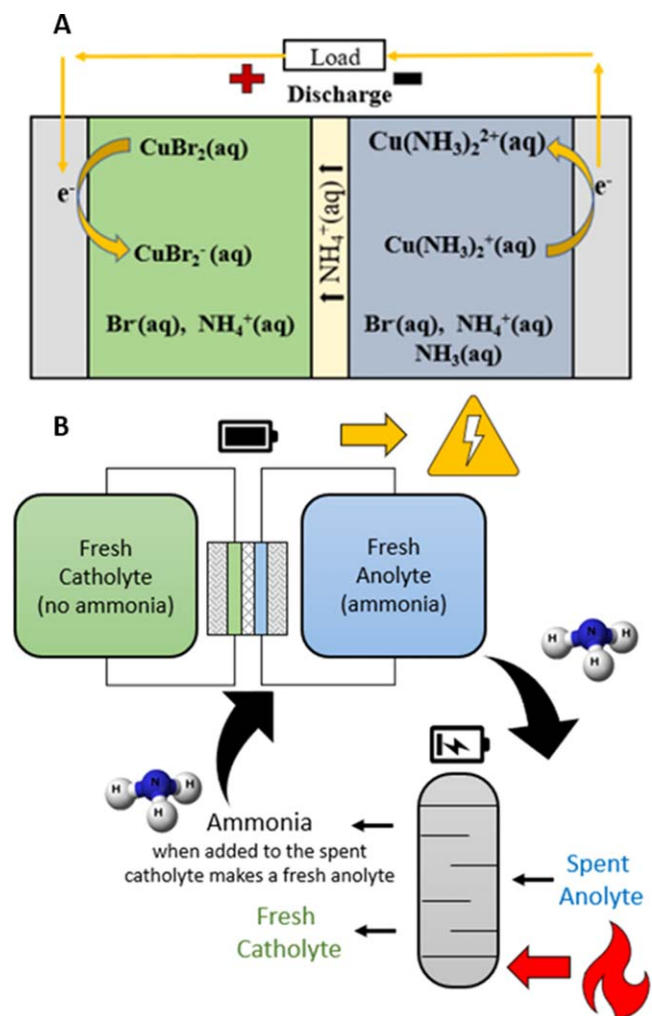


**Figure 2.** Electric discharge (A) and thermal charging process (B) for the all-aq TRAB.

equilibrium potentials of the new all-aq TRAB were significantly higher than single metal TRABs. Cu(I, II) equilibrium potentials ( $E_{eq}$ ) were quantified through OCP measurements which showed a connection between  $E^0$  and the participating metal-ligand complexes. The  $\text{NH}_3(\text{aq})$  solutions resulted in negative  $E_{eq}$  shifts, whereas  $\text{Br}^-(\text{aq})$  and  $\text{Cl}^-(\text{aq})$  solutions resulted in positive  $E_{eq}$  shifts. Increases in ligand concentration also increased the extent of the potential shift, as seen in Table I, where  $b_L$  is the ligand concentration ( $\text{mol kg}^{-1}$ ). Speciation calculations (See supplemental materials) showed that these potentials can be predicted with some accuracy if the reaction stability constants or the standard Gibbs energy of all species are known for both Cu(I) and Cu(II) complexation reactions. This is shown in Table I where  $E_{eq, \text{calculated}}$  are the resulting thermodynamic calculations with the Nernst equation using concentrations from the speciation calculations and their standard thermodynamic values as done previously.<sup>17,28</sup>

Speciation analyses showed that  $\text{Cl}^-(\text{aq})$  and  $\text{Br}^-(\text{aq})$  ligands preferentially bonded to Cu(I) species while  $\text{NH}_3(\text{aq})$  preferred Cu(II) species. Though speciation analyses generally agreed with experimental values obtained for both the  $\text{Br}^-(\text{aq})$  and  $\text{Cl}^-(\text{aq})$  species, Cu(II)- $\text{NH}_3(\text{aq})$  equilibrium constants from different sources<sup>25,29–34</sup> provided a large range of  $E_{eq}$  values suggesting some uncertainty surrounding the thermodynamic properties of Cu(II)- $\text{NH}_3(\text{aq})$  complexes. The use of Eq. 4 indicated that  $E_{eq}$  can be further increased to 0.79 V with additional  $\text{Br}^-(\text{aq})$  or decreased to  $-0.13 \text{ V}$ <sup>29</sup> with additional  $\text{NH}_3(\text{aq})$  by maximizing the extent of complexation.

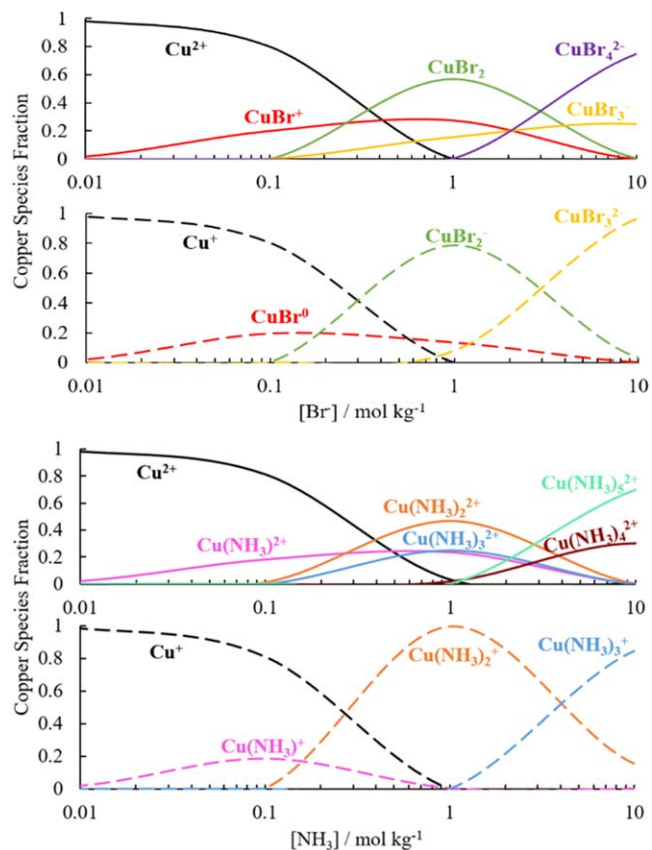


**Figure 3.** Fractional distribution of Cu(I, II)-Br and Cu(I, II)- $\text{NH}_3$  complexes as a function of total ligand concentration, at 25 °C and 1 bar with 0.5 mol  $\text{kg}^{-1}$  of total Cu.

**Table I.**  $E_{eq}$  values of the Cu(I,II) redox reaction with different ligand types and ligand concentrations ( $b_L$ ) for an equimolar solution of Cu(I, II) species.

Ligand	$b_L/\text{mol kg}^{-1}$	$E_{eq, \text{measured}}/\text{mV}$	$E_{eq, \text{calculated}}/\text{mV}$
$\text{NH}_3(\text{aq})$	1	$23 \pm 5$	52
	4	$-47 \pm 1$	-14
$\text{Cl}^-(\text{aq})$	1	$438 \pm 4$	447
	4	$543 \pm 7$	492
$\text{Br}^-(\text{aq})$	1	$518 \pm 1$	468
	4	$648 \pm 2$	533

Speciation diagrams (Fig. 3) were constructed using the equilibrium constants and the standard Gibbs energies at 25 °C and 1 bar to determine the species within the anolyte and catholyte. The speciation diagrams show that the dominant copper species complexes with more ligands as the ligand concentration increases in both the catholyte (copper bromide complexes) and anolyte (copper ammonia complexes) chambers. These diagrams are also advantageous for determining cathodic and anodic electrochemical half-reactions at specific concentrations, and ultimately establishing the electrochemical reaction order. The reaction order can lead to a distinction between the kinetic pathways involved in the Cu(I, II)-ligand reaction, but this will be further explored in future work.

**Electrochemical kinetics.**—The observed electrochemical kinetics of Cu(I, II) redox reactions were very fast compared to water electrolysis<sup>35</sup> and vanadium redox flow battery systems.<sup>36</sup> EIS was used to identify contributing mass and charge transfer resistances. Electrochemical kinetics and diffusion limitations were distinguished



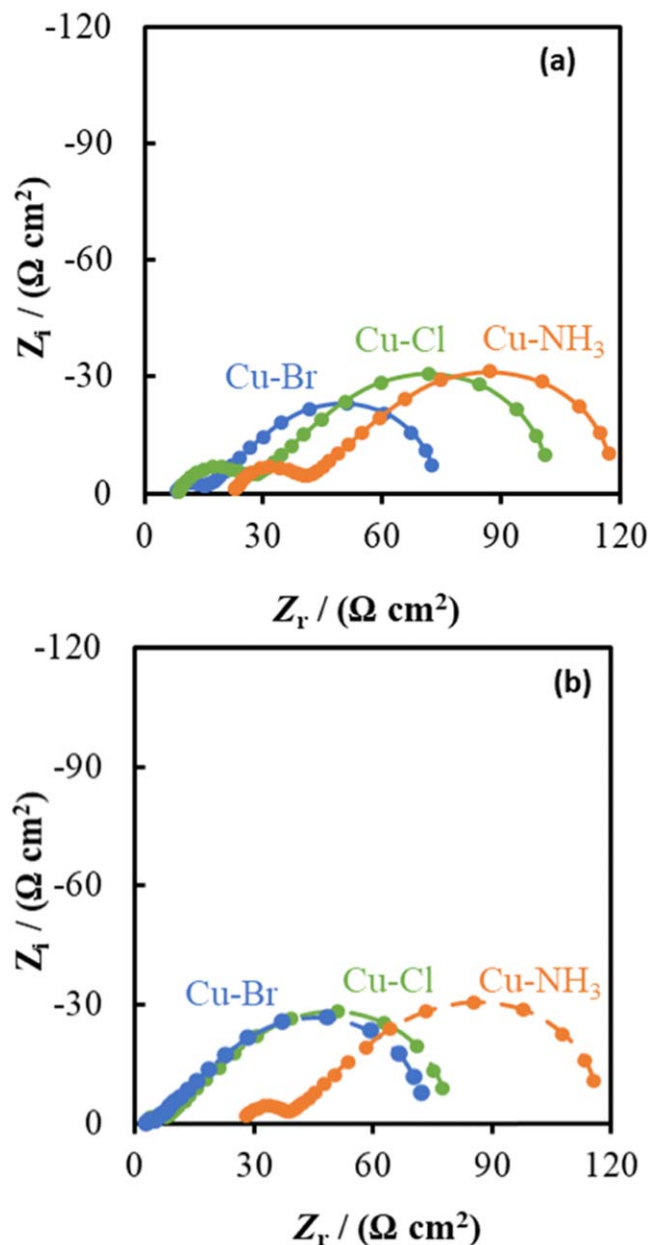


**Figure 4.** The effect of  $\text{NH}_3(\text{aq})$ ,  $\text{Cl}^-(\text{aq})$ , and  $\text{Br}^-(\text{aq})$  on the reaction kinetics and mass transfer sections of the impedance curves using the Pt working electrode at both (a)  $1 \text{ mol kg}^{-1}$ , (–), and (b)  $4 \text{ mol kg}^{-1}$ , (–), ligand concentrations. Conditions: 500 RPM,  $25^\circ\text{C}$  and 1 bar.

through their response to a changing diffusion layer thickness via RDE.<sup>17</sup> Varying rotation rates from 500 RPM to 2000 RPM dramatically decreased the low-frequency time constant (suggesting diffusion limitations) but did not impact the high-frequency time constant (indicating a surface reaction) (Fig. S3 (available online at [stacks.iop.org/JES/168/070523/mmedia](https://stacks.iop.org/JES/168/070523/mmedia))). EIS data (Fig. 4) from  $\text{NH}_3(\text{aq})$ ,  $\text{Br}^-(\text{aq})$ , and  $\text{Cl}^-(\text{aq})$  solutions were consistent with LSV data (Figure S4) in showing that the Cu(I, II) reactions were largely limited by mass transfer processes due to their fast kinetics. In addition to the effects of the electrode material (Fig. S2), the ligand concentration strongly altered  $R_{ct}$  values with  $\text{Br}^-(\text{aq})$ , and  $\text{Cl}^-(\text{aq})$  complexes but had little effect for  $\text{NH}_3(\text{aq})$  complexes (Fig. 4).

The rate constants,  $k_0$ , were determined using EIS and LSV data analysis methods<sup>20</sup> (See supplemental materials), indicating fast reaction kinetics with both Pt and GC electrodes (Table II). Rate constants were reported instead of the exchange current densities as

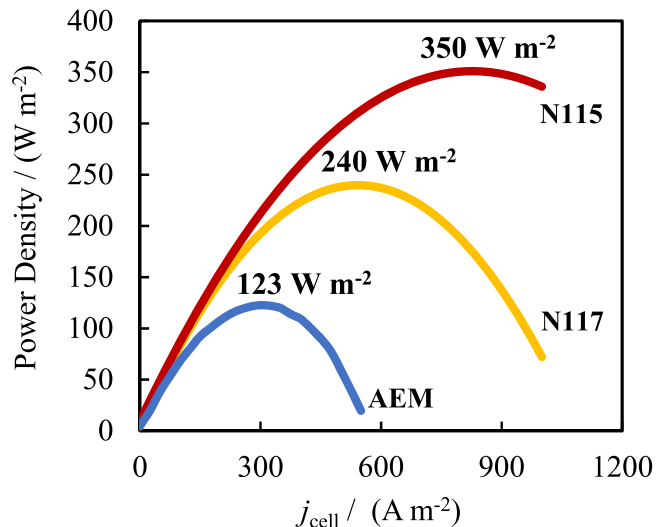


**Figure 5.** Power density curves obtained from the Br- $\text{NH}_3$  all-aq TRB with Nafion 117 (yellow), Nafion 115 (red) and AEM membrane (blue) at  $25^\circ\text{C}$  and 1 bar with  $0.5 \text{ mol kg}^{-1}$  of total copper.

**Table II.** ligand complexation impact on the  $k_0$  of the Cu(I, II) redox reaction for Pt and GC working electrode materials at  $25^\circ\text{C}$  and 1 bar.

Ligand	$b_L/\text{mol kg}^{-1}$	$k_{0,\text{GC}}/(\mu\text{m s}^{-1})$	$k_{0,\text{Pt}}/(\mu\text{m s}^{-1})$
$\text{NH}_3(\text{aq})$	1	$73 \pm 1$	$87 \pm 9$
	4	$87 \pm 2$	$101 \pm 5$
$\text{Cl}^-(\text{aq})$	1	$48 \pm 2$	$152 \pm 43$
	4	$87 \pm 1$	$360 \pm 113$
$\text{Br}^-(\text{aq})$	1	$59 \pm 5$	$293 \pm 51$
	4	$302 \pm 38$	$819 \pm 236$

they are independent of anodic and cathodic species concentrations. The small variations in  $k_0$  values between electrode materials with the Cu(I, II)- $\text{NH}_3(\text{aq})$  redox reaction suggest reactions may favor an outer-sphere charge transfer mechanism. In contrast, significant increases in  $k_0$  were observed with  $\text{Cl}^-(\text{aq})$  and  $\text{Br}^-(\text{aq})$  ligands, indicating inner-sphere charge transfer mechanisms and possibly ligand-bridging.<sup>37</sup>

Ligand-bridging has been observed with anion ligands that are both part of the oxidation and reduction metal ion coordination spheres and can lead to enhanced charge transfer rates.<sup>38</sup> Still, these rate constants are 10 to 100 times larger than those observed with vanadium redox reactions, which indicates that these reactions are highly suitable for electrochemical energy conversion systems.<sup>39</sup>

**Full cell performance.**—The fast kinetics and increased cell potentials resulted in high power densities from the all-aq TRAB (Fig. 5). Cation and anion-selective membranes were used to investigate which solution, catholyte or the anolyte, was more susceptible to ligand crossover as well as the impact on overall cell performance. Peak power densities obtained from the new flow battery chemistry were  $350 \text{ W m}^{-2}$  with N115,  $240 \text{ W m}^{-2}$  with N117, and  $123 \text{ W m}^{-2}$  with the AEM at  $20^\circ\text{C}$ . The power density curves were largely dominated by the ohmic losses regardless of the membrane tested and this is consistent with large  $j_0$  values observed from the RDE data as well as conductivity measurements obtained from full cell tests. A 44% increase in membrane thickness between the N115 and N117 membranes equated to a 46% decrease in peak power density, with an increasingly negative impact on the power density as  $j_{\text{cell}}$  increased. This highlights a proportional relationship between increased membrane thickness and a subsequent decrease in the power density of the cell.

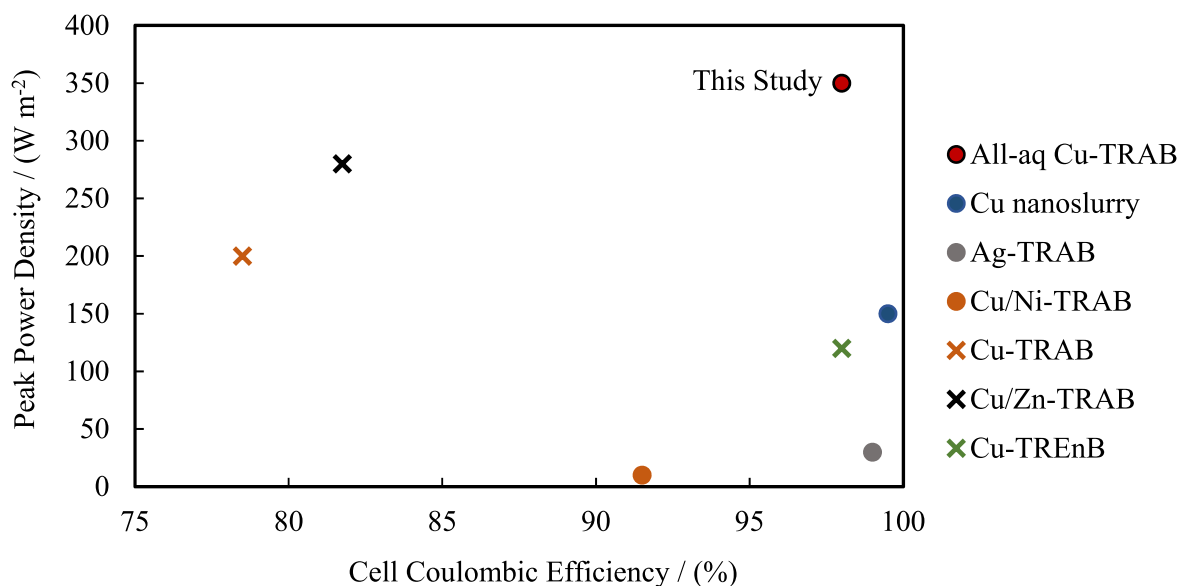


**Figure 6.** Comparison of peak power density and cell coulombic efficiency of different published TRB chemistries.<sup>2,5,14,46–48</sup> For metal-based batteries, the cell coulombic efficiency is an average of the reported electrode coulombic efficiencies. Circles indicate TRB chemistries that use reversible electrochemical reactions, and crosses indicate TRB chemistries with at least one irreversible electrochemical reaction.

Thermal recharging of the system was mimicked by the addition of  $\text{NH}_3(\text{aq})$  using a process developed previously.<sup>5</sup> Thermal regeneration has also been mimicked using ethylenediamine for Cu-based TRB chemistries.<sup>40</sup> The addition of ammonia to the positive electrolyte substituted the weak field strength ligand, effectively reducing the potential of the Cu(I, II) redox reaction, thereby forming the electrolyte at the negative electrode. This procedure established the maximum thermally rechargeable potential possible for the solutions used (i.e. assuming 100% recovery of ammonia). Relative to other flow batteries, such as the VRFB and Fe-Cr chemistries, the power densities obtained here of 123 to 350  $\text{W m}^{-2}$  are comparable to the 100 to 600  $\text{W m}^{-2}$  obtained from the more mature chemistries.<sup>41,42</sup> Similar ranges have been obtained, 100 to 300  $\text{W m}^{-2}$ , for some of novel organic and aqueous flow battery chemistries,<sup>43</sup> indicating that ligand tuning can provide a means to develop new flow battery chemistries from inexpensive materials. As seen from previous studies, the power densities obtained here at 25 °C, are expected to increase with elevated temperatures standard to flow battery operation.<sup>16,44</sup>

The coulombic efficiency was measured for the all-aq Cu(I, II) TRB at 25 °C and 1 bar was larger than those observed with copper metal TRABs. Electric charge-discharge cycling experiments were used to evaluate coulombic efficiency of the full cell with Eq. 5. This contrasts with previous metal TRAB chemistries where the coulombic efficiency of each electrode could be measured by simply measuring the change in mass of each electrode. The all-aq Cu-TRAB had a coulombic efficiency of 98% during the first cycle and then leveled at about 90% with successive cycles. With efficiencies above 90%, this was a clear improvement over the typical 35%–40% obtained with other metal copper-based systems (Fig. 6).<sup>5,45</sup>

The sustained, high cell coulombic efficiency of the all-aq Cu-TRAB indicates that the electrochemical reactions in each half of the cell are fully reversible. The decrease in efficiency seen after the first cycle was likely due to  $\text{NH}_3$  crossover through the membrane, which would decrease the performance of the catholyte over time. Evidence of  $\text{NH}_3$  crossover was based on the catholyte solution slowly changing from brown to blue during cycling. This crossover will have minimal impact on the TRAB performance, however, as the solutions are regenerated through thermal charging. While previous TRB publications were able to produce either high power cells or high coulombic efficiencies, few have been able to combine these two in the same chemistry. Therefore, the all-aq Cu-TRAB is unique because it can produce high power densities with high

coulombic efficiencies using the same low-cost materials that have been used previously.

Energy storage densities possible with the all-aq Cu-TRAB were also larger than those observed with previously published TRAB chemistries. With a standard cell potential of about 0.7 V and stable electroactive species concentrations of at least 0.5  $\text{mol kg}^{-1}$ , the energy storage density of the new TRAB was estimated to be at least 9.4  $\text{Wh L}^{-1}$  using Eq. 5. This is considerably higher than the current values of 2.4  $\text{Wh L}^{-1}$  from Cu-TRABs<sup>2</sup> and 1.2  $\text{Wh L}^{-1}$  from Ag-TRABs.<sup>5</sup>

## Conclusions

A new all-aqueous thermally regenerative redox flow battery was developed with favorable performance parameters relative to previous TRAB chemistries. A series of RDE experiments demonstrated that the new chemistry had a large equilibrium potential with fast charge-transfer kinetics. The strong field strength ligand  $\text{NH}_3(\text{aq})$  resulted in a decrease of  $E_{\text{eq}}$  for the Cu (I, II) reaction to  $-47 \pm 1$  mV vs SHE whereas the weak field strength ligands,  $\text{Cl}^-(\text{aq})$  and  $\text{Br}^-(\text{aq})$ , increased the  $E_{\text{eq}}$  by  $516 \pm 7$  mV and  $638 \pm 2$  mV vs SHE. Quantification of  $k_0$  values indicated that these reactions were fast regardless of the ligand species. Interestingly, the small variation in  $k_0$  between Pt and GC working electrodes for  $\text{NH}_3(\text{aq})$ -based complexes suggests that it followed an outer-sphere charge transfer mechanism, whereas  $\text{Cl}^-(\text{aq})$  and  $\text{Br}^-(\text{aq})$  showed drastic differences in  $k_0$  pointing to inner-sphere reaction mechanisms. Peak power densities obtained from the new battery chemistry were 350  $\text{W m}^{-2}$  using a N115 membrane, exceeding previous TRAB technologies and putting them on par with power densities obtained from conventional redox flow battery chemistries. Coulombic efficiencies over 90% and an energy storage density of at least 9.4  $\text{Wh L}^{-1}$  from the new chemistry were significant improvements over existing chemistries which demonstrates promising advances to the performance of TRABs.

## ORCID

Derek M. Hall  <https://orcid.org/0000-0001-9648-596X>

## References

1. M. Rahimi, A. P. Straub, F. Zhang, X. Zhu, M. Elimelech, C. A. Gorski, and B. E. Logan, *Energy Environ. Sci.*, **11**, 276 (2018).
2. V. M. Palakkal, T. Nguyen, P. Nguyen, M. Chernova, J. E. Rubio, G. Venugopalan, M. Hatzell, X. Zhu, and C. G. Arges, "High Power Thermally Regenerative

- Ammonia-Copper Redox Flow Battery Enabled by a Zero Gap Cell Design, Low-Resistant Membranes, and Electrode Coatings." *ACS Appl. Energy Mater.*, **3**, 4787 (2020).
3. S. Brueske, R. Sabouni, C. Zach, and H. Andres, *Manufacturing Energy and Carbon Footprints (2010 MECS)*, U.S. DOE Office of Energy Efficiency & Renewable Energy 184 (2012), <http://energy.gov/eere/amo/manufacturing-energy-and-carbon-footprints-2010-mecs>.
  4. "Energy Policies of IEA Countries: United States 2019 Review." IEA (2019), <https://www.iea.org/reports/energy-policies-of-iea-countries-united-states-2019-review>.
  5. M. Rahimi, T. Kim, C. A. Gorski, and B. E. Logan, *J. Power Sources*, **373**, 95 (2018).
  6. K. Braimakis, M. Preißinger, D. Brüggemann, S. Karellas, and K. Panopoulos, *Energy*, **88**, 80 (2015).
  7. D. Enescu, *Green Energy Advances* (IntechOpen, London) (2019).
  8. A. Bianchini, M. Pellegrini, and C. Saccani, *Energy Procedia* (Elsevier, Amsterdam) **45**, 268 (2014).
  9. S. M. Jung, J. Kwon, J. Lee, K. Shim, D. Park, T. Kim, Y. H. Kim, S. J. Hwang, and Y. T. Kim, *ACS Appl. Energy Mater.*, **3**, 6383 (2020).
  10. W. Wang, H. Tian, G. Shu, D. Huo, F. Zhang, and X. Zhu, *J. Mater. Chem. A*, **7**, 5991 (2019).
  11. B. Orr, B. Singh, L. Tan, and A. Akbarzadeh, *Appl. Therm. Eng.*, **73**, 588 (2014).
  12. W. Wang, G. Shu, H. Tian, and X. Zhu, "A bimetallic thermally-regenerative ammonia-based flow battery for low-grade waste heat recovery." *Power Sources*, **424**, 184 (2019).
  13. A. Xie and S. C. Papat, *Chem. Eng. J. Adv.*, **3**, 100020 (2020).
  14. M. Rahimi, A. D'Angelo, C. A. Gorski, O. Scialdone, and B. E. Logan, *J. Power Sources*, **351**, 45 (2017).
  15. M. Rahimi, A. P. Straub, F. Zhang, X. Zhu, M. Elimelech, C. A. Gorski, and B. E. Logan, *Energy Environ. Sci.*, **11**, 276 (2018).
  16. W. Wang, D. Huo, H. Tian, X. Zhu, and G. Shu, *Electrochim. Acta*, **357**, 136860 (2020).
  17. D. M. Hall, N. N. Akinfiev, E. G. LaRow, R. S. Schatz, and S. N. Lvov, *Electrochim. Acta*, **143**, 70 (2014).
  18. S. Khurana, D. M. Hall, R. S. Schatz, and S. N. Lvov, *ECS Electrochem. Lett.*, **4**, F21 (2015).
  19. D. M. Hall, J. R. Beck, and S. N. Lvov, *Electrochem. Commun.*, **57**, 74 (2015).
  20. D. M. Hall, E. G. LaRow, R. S. Schatz, J. R. Beck, and S. N. Lvov, *J. Electrochem. Soc.*, **162**, F108 (2015).
  21. D. M. Hall and S. N. Lvov, *Electrochim. Acta*, **190**, 1167 (2016).
  22. P. Vanysek, *CRC Handbook of Chemistry and Physics*, **1015-88-5-89** (2020).
  23. J. W. Johnson, E. H. Oelkers, and H. C. Helgeson, *Comput. Geosci.*, **18**, 899 (1992).
  24. B. E. Etschmann, J. R. Black, P. V. Grundler, S. Borg, D. Brewre, D. C. McPhail, L. Spiccia, and J. Brugger, *RSC Adv.*, **1**, 1554 (2011).
  25. Lange, N. Adolph, *Lange's Handbook of Chemistry*, **15**, 1217 (1998).
  26. C. Ponce de León, A. Frías-Ferrer, J. González-García, D. A. A. Szánto, and F. C. C. Walsh, *J. Power Sources*, **160**, 716 (2006).
  27. D. M. Hall, J. Grenier, T. S. Duffy, and S. N. Lvov, *J. Electrochem. Soc.*, **167**, 110536 (2020).
  28. D. M. Hall, J. R. Beck, E. Brand, M. Ziomek-Moroz, and S. N. Lvov, *Electrochim. Acta*, **221**, 96 (2016).
  29. B. J. Hathaway and A. G. Tomlinson, *Coord. Chem. Rev.*, **5**, 1 (1970).
  30. P. Kamau and R. B. Jordan, *Inorg. Chem.*, **40**, 3879 (2001).
  31. OLI, (2020), OLI Systems Inc..
  32. E. A. Stricker, "Cuprous Bromide Electrochemistry and its Application in a Flow Battery." *Electronic Thesis*, Case Western Reserve University (2019), [https://etd.ohiolink.edu/apexprod/rws\\_etd/send\\_file/send?accession=case1546604124529032&disposition=inline](https://etd.ohiolink.edu/apexprod/rws_etd/send_file/send?accession=case1546604124529032&disposition=inline).
  33. S. Dhillon and R. Kant, *J. Chem. Sci.*, **129**, 1277 (2017).
  34. Z. Ahmad, *Principles of Corrosion Engineering and Corrosion Control* (Elsevier, Amsterdam) 1st ed. (2006).
  35. S. N. Lvov, *Introduction to Electrochemical Science and Engineering* (CRC Press, Florida, FL) 1st ed. (2014).
  36. J. Kim and H. Park, *Appl. Energy*, **206**, 451 (2017).
  37. A. J. Bard and L. R. Faulkner, *Electrochemical methods: fundamentals and applications* (Wiley, New York, NY) 2nd ed. (2000).
  38. A. Haim, "Role of the bridging ligand in inner-sphere electron-transfer reactions." *Accounts of Chemical Research*, **8**, 264 (1975).
  39. M. Liu, Z. Xiang, H. Deng, K. Wan, Q. Liu, J. Piao, Y. Zheng, and Z. Liang, *J. Electrochem. Soc.*, **163**, H937 (2016).
  40. M. Rahimi, L. Zhu, K. L. Kowalski, X. Zhu, C. A. Gorski, M. A. Hickner, and B. E. Logan, *J. Power Sources*, **342**, 956 (2017).
  41. Y. K. Zeng, X. L. Zhou, L. An, L. Wei, and T. S. Zhao, *J. Power Sources*, **324**, 738 (2016).
  42. D. S. Aaron, Q. Liu, Z. Tang, G. M. Grim, A. B. Papandrew, A. Turhan, T. A. Zawodzinski, and M. M. Mench, *J. Power Sources*, **206**, 450 (2012).
  43. H. Chen, G. Cong, and Y. Lu, *J. Energy Chem.*, **27**, 1304 (2018).
  44. C. Zhang, T. S. Zhao, Q. Xu, L. An, and G. Zhao, *Appl. Energy*, **155**, 349 (2015).
  45. F. Zhang, N. LaBarge, W. Yang, J. Liu, and B. E. Logan, *ChemSusChem*, **8**, 1043 (2015).
  46. W. Wang, G. Shu, H. Tian, D. Huo, and X. Zhu, *J. Power Sources*, **424**, 184 (2019).
  47. Y. Shi, L. Zhang, J. Li, Q. Fu, X. Zhu, and Q. Liao, *Renew. Energy*, **159**, 162 (2020).
  48. S. Maye, H. H. Girault, and P. Peljo, *Energy Environ. Sci.*, **13**, 2191 (2020).